Int. J. Electrochem. Sci., 16 **(2021)** Article Number: 211038, doi: 10.20964/2021.10.44

International Journal of
ELECTROCHEMICAL
SCIENCE
www.electrochemsci.org

Study on Corrosion Resistance of AZ31 Magnesium Alloy Coated with Graphene Modified Epoxy and Polyurethane Coatings

Zhengyuan Gao, Chengjin Sun, Dong Yang, Lianteng Du, Xiang Zhang, Pengfei Sun[*]

School of Mechatronics and Automotive Engineering, Chongqing Jiaotong University, Chongqing 400074, China
[*]E-mail: danny25@163.com

Received: 22 June 2021 / *Accepted:* 9 August 2021 / *Published:* 10 September 2021

Graphene-modified epoxy resin coating can impart better corrosion resistance to magnesium alloys. In this regard, the present work focuses on the preparation of graphene-modified oil-based epoxy resin/polyurethane composite coating (G/OEP/OPU) and waterborne epoxy resin/polyurethane composite coating (G/WEP/WPU) and is coated over the AZ31 magnesium alloy to elucidate the corrosion protection behavior. Scanning electron microscopic observation shows that the surface quality of graphene flakes is good. When graphene is added to the oil-based and waterborne epoxy primers, the surface quality of the oil-based polyurethane topcoat is improved, while the surface quality of the waterborne polyurethane topcoat is reduced. Fourier transform infrared spectroscopic testing shows that the coating and the curing agents are the major structural components of the coating. The electrochemical test results show that the composite coatings can significantly improve the corrosion resistance of magnesium alloys. In the oily composite coatings, G/OEP/OPU-0.3wt% shows the highest corrosion resistance where the corrosion current density is 1.81×10^{-12}A/cm^2. For waterborne composite coatings, G/WEP/WPU-0wt% has the least corrosion current density value of 5.07×10^{-12} A/cm^2. The comprehensive analysis suggests that the graphene improves the bonding performance of the primer and topcoat in the case of oily composite coating leading to the improvement in the surface quality of the topcoat and increase the coating's ability to resist the penetration of corrosive media. For waterborne composite coatings, the hydrophobic graphene improves the hydrophobicity of the primer coat, and therefore, the curing quality of the waterborne polyurethane topcoat is deprived that weakens the corrosion resistance of the waterborne composite coating.

Keywords: AZ31 magnesium alloy, graphene, epoxy primer, polyurethane topcoat, corrosion resistance

1. INTRODUCTION

Magnesium alloys are widely used to design lightweight structures in industries that indirectly save energy and reduces emission [1-4]. However, the standard electrode potential of magnesium alloys

is relatively low, and therefore, they are easily oxidized leading to design failure. Oxides have a high degree of porosity and are loosely packed which makes it impossible to effectively shield water and air from the environment. As a consequence, the corrosion resistance of magnesium alloys is found to be poor [5,6].

Recently, many articles have been reported that uses graphene and its derivatives to modify the epoxy resin coatings to enhance the corrosion resistance of magnesium alloys [7-10]. As epoxy resin is an organic coating, it is easy to prepare, cost-effective, and possesses many advantages. From many years of application research, two types of coatings have been developed as oily and waterborne coatings. Oil-based epoxy resin has better film-forming properties but easily causes environmental pollution. Waterborne epoxy resins are easy to clean and harmless to the environment but have poor water resistance. Affected by the curing and crosslinking performance, the coating is prone to defects such as holes that occurred during the curing process. Therefore, many researchers have been using graphene as corrosion inhibitor fillers to further improve the corrosion resistance of the epoxy coating. Graphene can fill up the defects generated during the curing process of the coating through its inherent higher specific surface area with 2D structure and has a strong shielding performance against corrosive media.

In real-time industrial applications, for efficient corrosion protection offered by the epoxy coating to the substrate, it is often used as a primer and a polyurethane topcoat is applied to its surface. This design not only reduces the wear during use but also achieves a certain aesthetic effect. However, most of the current research simply uses graphene to modify the single-layer elasticity and surface to improve the corrosion resistance of the epoxy coating [11-15]. However, there is no comprehensive analysis of the effect of graphene-modified epoxy primer on the overall performance of epoxy/polyurethane composite coating. In this context, the present work focuses on the preparation and effectiveness of graphene-modified oily and waterborne epoxy/polyurethane composite coatings to be used as corrosion-resistant coating for AZ31 magnesium alloys to explore the effect of composite coatings on the corrosion resistance of composite coated magnesium alloys.

2. EXPERIMENTAL

2.1. Materials

AZ31 wrought magnesium alloy is selected as the base material for this work. The chemical compositions of the alloy are shown in Table 1.

Table 1. Chemical compositions of AZ31 magnesium alloy/ wt.%

Element	Al	Zn	Mn	Cu	Ni	Fe	Mg
Content	3.007	1.054	0.488	0.001	0.002	0.004	Bal.

The samples are cut from a block of AZ31 magnesium alloy using an electro-discharge machine (EDM) with dimensions of 20×20×10 mm^3.Before the experiments, the specimens will be polished step

by step with alumina abrasive sandpaper up to 3000 mesh, and cleaned with acetone and alcohol solution.

The oil-based bisphenol A epoxy primer, oil-based aliphatic polyurethane topcoat and the corresponding curing agent are purchased from Guangzhou Tuan Anti-corrosion Technology Co., Ltd.. The waterborne phenolic epoxy topcoat, waterborne acrylic polyurethane topcoat and corresponding curing agent are purchased from Chongqing Xihelong Chemical Technology Co., Ltd..

2.2. Coating preparation

At first, epoxy primer is prepared to coat on the surface of the AZ31 magnesium alloy for which a known quantity of graphene is mixed with 50 g of oil-based and waterborne epoxy resin paint. The proportion of graphene with respect to the mass of the epoxy resin paint is 0 wt.%, 0.1 wt.%, 0.3 wt.%, and 0.6 wt.%. The mixture is then stirred for 30 min under high-speed stirring to uniformly mix the graphene in the paint matrix. The above mixture is then added with the corresponding curing agent, wherein the mass ratio of the oil-based epoxy resin to the curing agent is 3:1 and the mass ratio of the waterborne epoxy resin to the curing agent is 5:1. To ensure uniform dispersion of curing agent, mechanical stirring is employed. Subsequently, oily and waterborne epoxy resin primers modified with different graphene proportions are brush coated over the surface of the AZ31 magnesium alloy and cured at room temperature for 7 days. After complete curing, the polyurethane topcoat is prepared by mixing it with the curing agent. The mass ratio of oily polyurethane topcoat and curing agent is fixed at 3:1 and the mass ratio of waterborne polyurethane topcoat and curing agent is 5:1. The polyurethane topcoat and curing agent are mechanically stirred till the mixture is uniformly mixed. Subsequently, oil-based and waterborne polyurethane topcoats are applied over the cured oil-based and waterborne epoxy primers respectively.

For convenience, the graphene-modified oil-based epoxy resin/polyurethane composite coatings are designated as G/OEP/OPU-0wt%, G/OEP/OPU-0.1wt%, G/OEP/OPU-0.3wt%, and G/OEP/OPU-0.6wt% whereas the graphene-modified waterborne epoxy/polyurethane composite coatings are designated as G/WEP/WPU-0wt%, G/WEP/WPU-0.1wt%, G/WEP/WPU-0.3wt %, and G/WEP/WPU-0.6wt%.

The JSM-6610 scanning electron microscope is used to observe the microscopic morphology of graphene and the coatings. Raman spectroscopy is used to characterize and analyze graphene. Fourier transform infrared (FT-IR) spectroscopy is used to analyze the internal chemical bonds present in the coating where the specific working parameters such as the wavenumber range and the resolution is set as 4000 cm^{-1} to 400 cm^{-1}, and 4 cm^{-1} respectively. The corrosion resistance behavior of bare and coated magnesium alloy is elucidated using an electrochemical workstation (CHI660E series). In the test system, the substrate i.e., bare or coated magnesium alloy is used as the working electrode (test area is 1 cm^2), the platinum electrode is the counter electrode, and the saturated calomel electrode is the reference electrode where 3.5 wt.% NaCl solution is used as the test corrosive medium; all the tests are performed at room temperature. The open circuit potential (OCP) test is used to clarify the stability of the tested sample system. The specific test parameters are fixed where the scanning range is -3 V to 1 V and the scan rate is 1 mV/s.

3. RESULTS AND DISCUSSION

3.1. Characterization of graphene and coatings

The morphology of graphene is observed from the microscopic images shown in Figure 1. From the low magnification image, it is inferred that the graphene flakes are mutually attracted by the π-π bonds leading to stacking and agglomeration where the size of the agglomerates is in the range 10-20 μm. Also, there are a few single-layer graphene flakes scattered on the side, with a size of about 5μm. Figure 1(b) shows the surface morphology of graphene under high magnification where some wrinkles and few defects are observed. In terms of structure, it shows strong shielding performance against corrosive media.

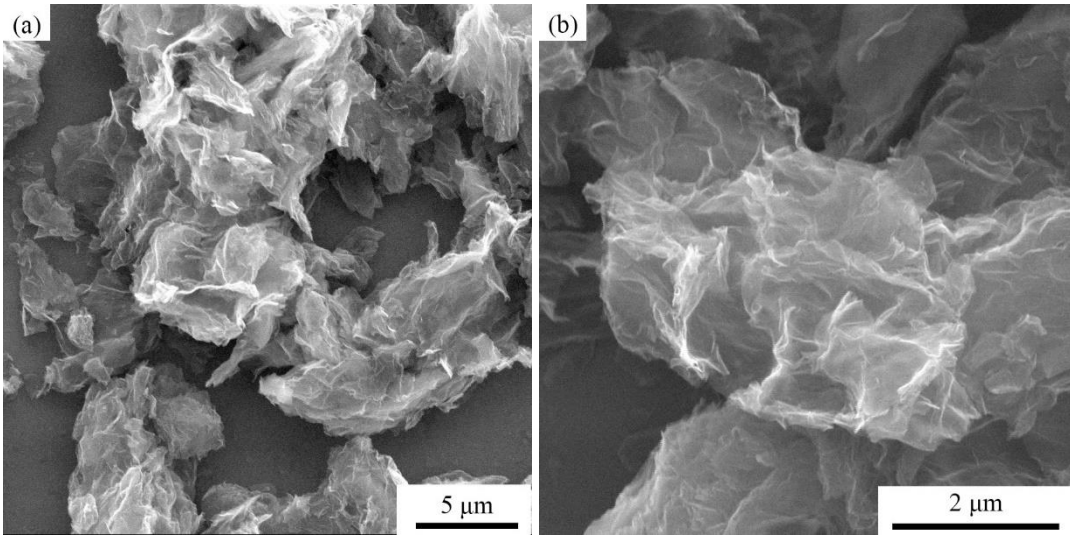

Figure 1. Graphene micro morphology under different magnifications

The Raman spectrum of graphene is recorded and is shown in Figure 2. From the figure, it is found that the typical three peaks of graphene, namely D peak (1342 cm^{-1}), G peak (1578cm^{-1}), and 2D peak (2691 cm^{-1}) are present. The D peak is originated from the stretching vibration of the sp2 hybrid carbon atoms of graphene attributed to the disordered arrangement of the carbon lattice and the surface defects of the graphene. The G peak in the Raman spectrum is generated by the in-plane vibration of graphene sp^2 hybrid carbon atoms. The number of stacked layers of graphene flakes will have an impact on the intensity of the G peak. Therefore, the number of stacked layers of graphene can be estimated from the intensity of the G peak. The presence of a 2D peak substantiates that the two photonic lattices vibrate, which is the frequency-doubled peak of the D peak. However, the difference is that the 2D peaks are not related to the disordered arrangement of the carbon lattice and the surface defects of the graphene [16,17].

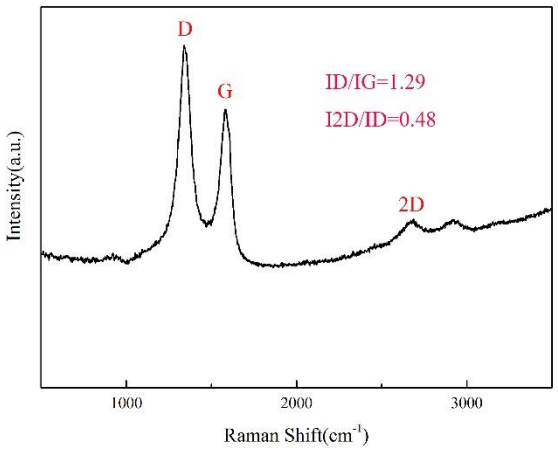

Figure 2. Graphene Raman test spectrum

From the peak intensities, the ID/IG ratio and the I2D/IG ratio are calculated as 1.29 and 0.48 respectively. From the calculation, it is clear that the G band of a graphene layer is stronger than the 2D band. But on the contrary, when the number of graphene layers is more than two, the 2D band should be stronger than the G-band. And as the number of layers increases greater than five, the 2D peak will move to a higher wavenumber and becomes extremely uneven. Through the ratio of the 2D peak to the G peak and the 2D peak shape, it can be inferred that the number of stacked layers of graphene is between 3 - 6 layers [18,19].

The FT-IR spectra of the oil-based epoxyoil-based epoxy/polyurethane coatings with different graphene content are shown in Figure 3(a). The characteristic absorption peaks of carbonyl and C-O-C bonds are observed at 1710 cm^{-1} and 1725 cm^{-1}, respectively. The weak absorption peaks in the wavenumber region of 3400 cm^{-1} - 3500 cm^{-1} are observed for all four spectra which are caused by the stretching vibrations of -NH and -OH. The symmetric and asymmetric vibration absorption peaks of methylene appear at 2800 cm^{-1} and 2900 cm^{-1}, respectively. The band observed at 1470 cm^{-1} corresponds to the deformation vibration of $-CH_2$. The band observed at 1380 cm^{-1} corresponds to the symmetrical vibration of $-CH_3$. The absorption peaks at the 1250 cm^{-1} and 1145 cm^{-1} bands correspond to the stretching vibration of the C-O bond and the stretching vibration of the C-O-C bond, respectively [20,21].

The FT-IR spectra of the waterborne epoxy/polyurethane coatings with different graphene content are shown in Figure 3(b). The absorption vibrational peaks of the C=O bond and N-H bond from the polyurethane main chain appear at 1690 cm^{-1} and 1480 cm^{-1}, respectively. The absorption peaks observed at 3250 cm^{-1} - 3500 cm^{-1} are caused by the stretching vibrations of -NH and -OH. The two absorption peaks at 2860 cm^{-1} and 2940 cm^{-1} are attributed to the deformation vibration of $-CH_2$ and the symmetrical vibration of $-CH_3$, respectively. The vibration absorption peak corresponding to C=O is located at 1701 cm^{-1} [15,22].

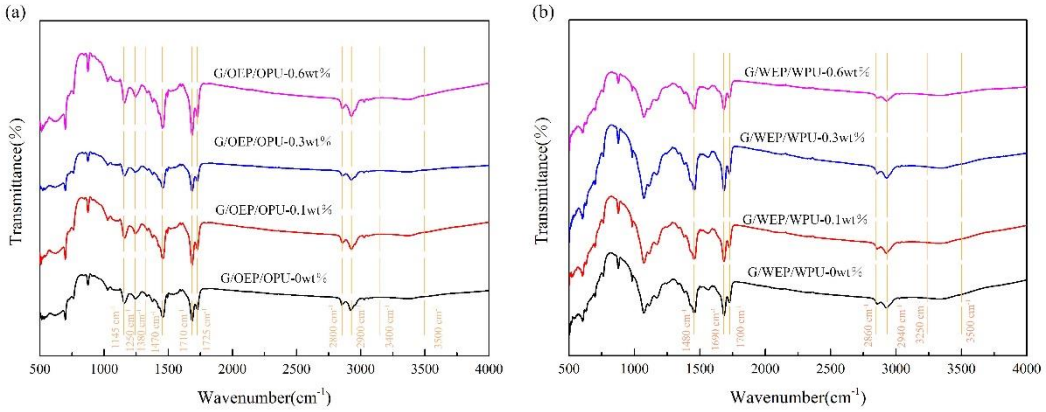

Figure 3. Infrared spectra of graphene modified epoxy/polyurethane composite coatings: (a) oil-based epoxy/polyurethane coating and (b) waterborne epoxy/polyurethane coating

3.2. Morphologies and corrosion resistance of graphene modified coatings

Figure 4 shows the surface morphologies of the graphene-modified oil-based epoxy resin/polyurethane coatings. It can be seen from the figures that as the graphene content in the primer increases, the surface quality of the polyurethane topcoat gradually improves. When the graphene content of the primer is 0.3 wt.%, the surface quality reaches its best state. However, while the graphene content increases to 0.6 wt.%, the surface quality starts deteriorating. From the obtained results, it is clear that the surface properties of the primer greatly influence the surface finish of the topcoat. In the absence of graphene (0 wt.%), the cured epoxy primer displays large surface defects and is accompanied by pore formation. These defects induce a negative impact on the polyurethane curing process, causing an uneven spreading of polyurethane over the surface of the cured primer. As a result, the surface roughness of the topcoat is increased and the cross-linking of the chemical bonds i.e., curing of the coating is hindered which influences the curing quality of the coating. It can be observed from Figure 4(a) that the coating surface began to flake off and causes pit formation which is accompanied by a more serious blistering effect. However, it is inferred that while the surface quality of the cured primer improves, the surface quality of the polyurethane topcoat has also improved consequently. This phenomenon can be observed in Figure 4(b). As the graphene content of the primer increases, the surface quality of the oil-based epoxy coating itself is improved. The surface defects of the polyurethane topcoat have diminished where the initial flaky peeling behavior is altered to the slight cracking in some places, the pits are almost disappeared, and only a minimal blistering effect is noticed. When the graphene content of the primer reaches 0.3 wt.%, the polyurethane coating achieves the best surface quality displaying no peeling and pits on the coating surface [Figure 4c]. However, when the graphene content of the primer is increased to 0.6 wt.%, the surface quality of the primer is reduced owing to the agglomeration of the graphene flakes in the primer [Figure 4d]. These agglomerations facilitate the generation of granular protrusions on the surface of the polyurethane topcoat, resulting in a declined surface finish.

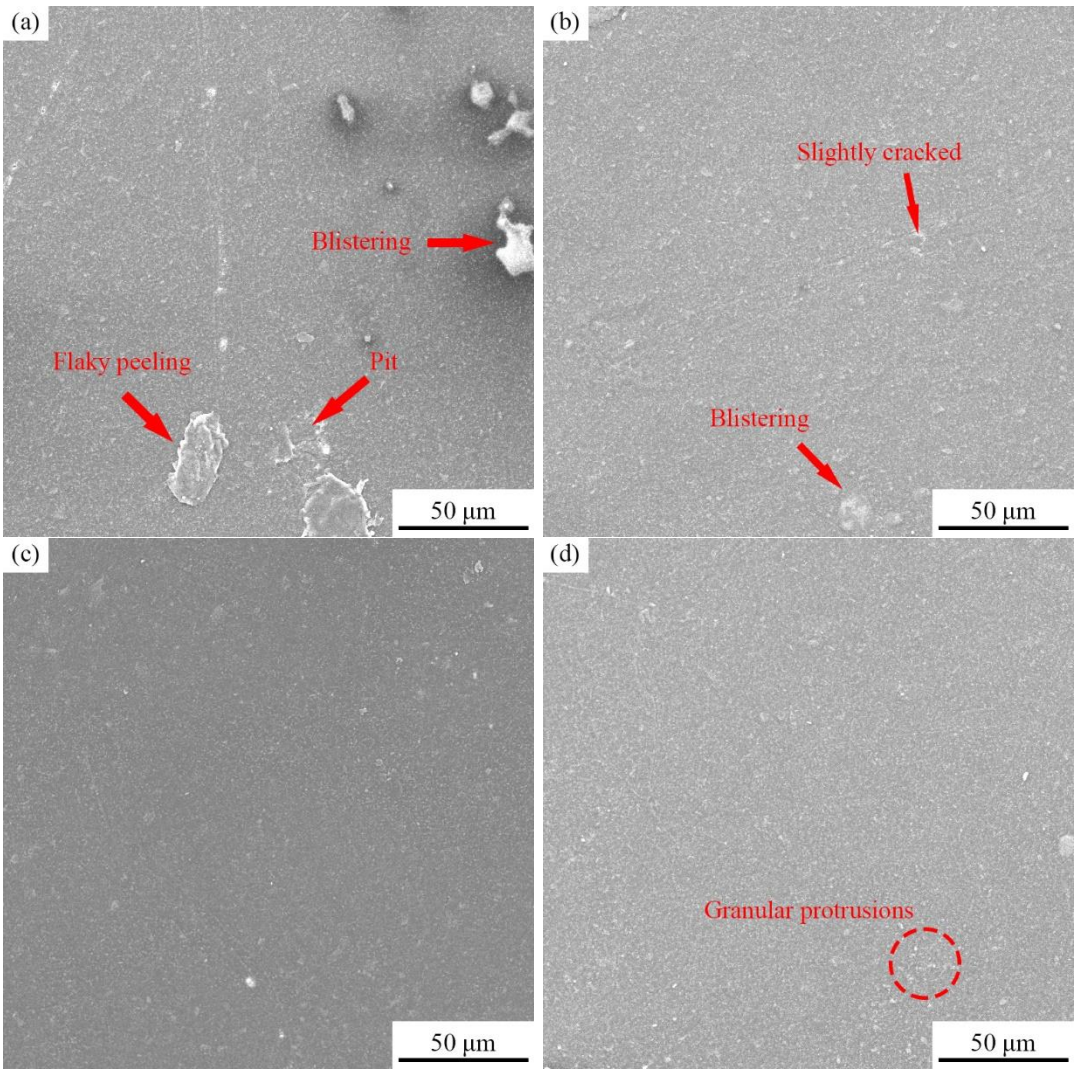

Figure 4. Surface microscopic images of graphene modified oil-based epoxy/polyurethane coatings, (a) G/OEP/OPU-0wt%, (b) G/OEP/OPU-0.1wt%, (c) G/OEP/OPU-0.3wt%, and (d) G/OEP/OPU-0.6wt%

Figure 5 shows the microscopic surface morphologies of the graphene-modified waterborne epoxy/polyurethane composite coatings. It can be validated from the figures that as the graphene content in the epoxy primer increases, the surface quality of the polyurethane topcoat gradually decreases. When graphene is not added to the waterborne epoxy primer, the polyurethane topcoat exhibits the best surface quality feature [Figure 5(a)]. On contrary, as the graphene content increases to 0.1 wt.% [Figure 5b], 0.3 wt.% [Figure 5c], and 0.6 wt.% [Figure 5d], it is inferred that when graphene is added to the waterborne epoxy primer granular protrusions begins to appear in the coating inducing improvement in the surface roughness. Consequently, the increase in graphene content deteriorates the surface quality of the polyurethane topcoat. When the graphene content in the waterborne epoxy primer reaches 0.6 wt.%, serious blistering and peeling begin to appear on the polyurethane topcoat. This behavior is caused owing to the high hydrophobicity of graphene flakes. As graphene is added as the slow-release filler to the waterborne epoxy resin coating, it will improve the hydrophobic behavior of the cured primer surface.

When waterborne polyurethane is coated over the hydrophobic graphene-modified waterborne epoxy primer, the higher hydrophobicity of the primer hinders its interaction with the topcoat since the dispersion medium of the waterborne polyurethane topcoat is water. Therefore, the waterborne topcoat is unable to spread evenly on the surface of the graphene-modified waterborne epoxy primer. Hence, the internal stress of the coating grows, declining the surface quality of the waterborne polyurethane coating.

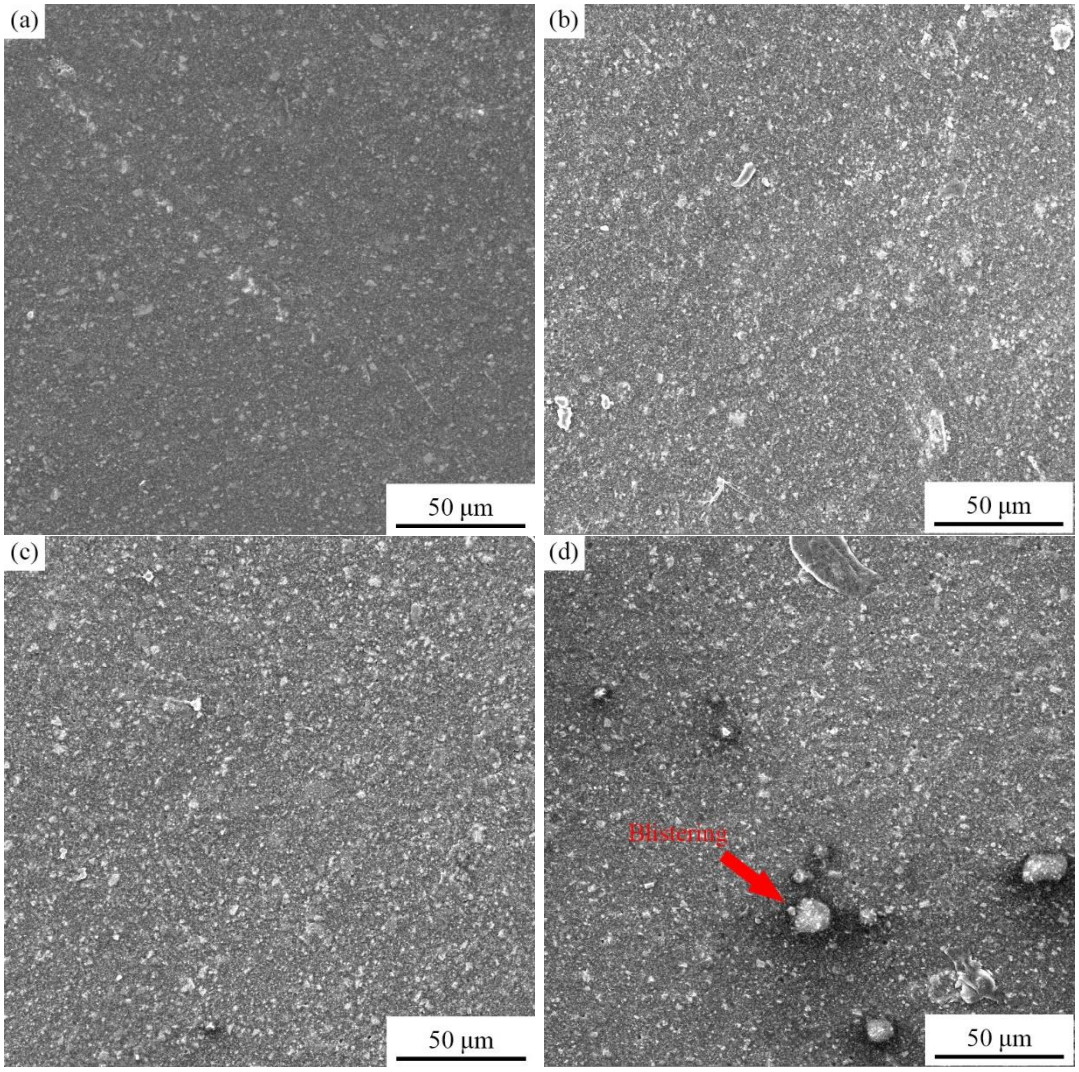

Figure 5. Microscopic surface morphologies of graphene-modified waterborne epoxy/polyurethane coatings, (a) G/WEP/WPU-0wt%, (b) G/WEP/WPU-0.1wt%, (c) G/WEP/WPU-0.3wt%, and (d) G/WEP/WPU-0.6wt%

Figure 6 shows the potentiodynamic polarization curves of the graphene-modified oily and waterborne epoxy/polyurethane composite coatings from which specific electrochemical parameters are derived and summarized in Table 2. As the corrosion potential is greatly influenced by environmental factors, the present study uses the corrosion current density values to evaluate the corrosion resistance of the coated magnesium alloys. The smaller the corrosion current density value, the higher the corrosion

resistance. Comprehensive observations substantiate that the coating can significantly improve the corrosion resistance of magnesium alloys.

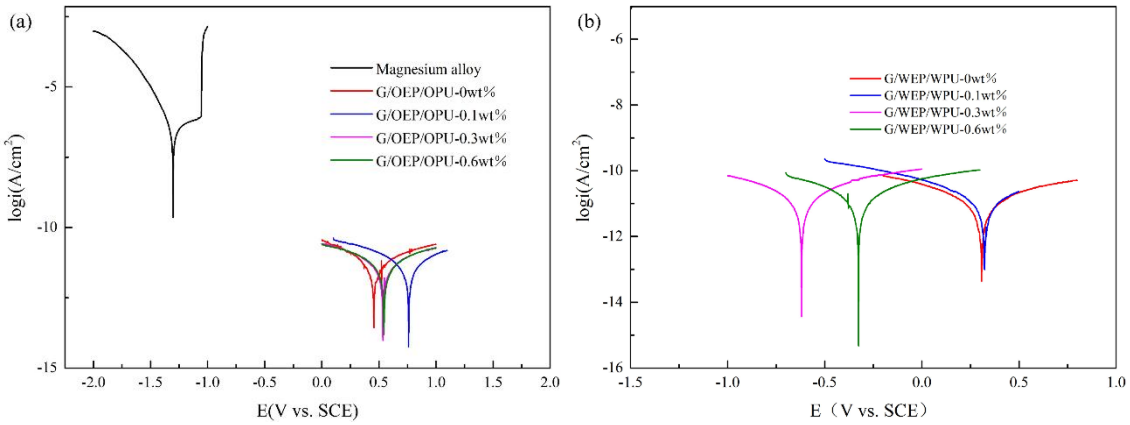

Figure 6. Potentiodynamic polarization curves of magnesium alloy and coatings

Table 2. Potentiodynamic polarization curves related parameters

Sample	Corrosion current density （A/cm^2）	Corrosion potential （V）
Magnesium alloy	2.96×10^{-7}	-1.303
G/OEP/OPU-0wt%	2.37×10^{-12}	0.455
G/OEP/OPU-0.1wt%	2.15×10^{-12}	0.760
G/OEP/OPU-0.3wt%	1.81×10^{-12}	0.535
G/OEP/OPU-0.6wt%	1.86×10^{-12}	0.544
G/WEP/WPU-0wt%	5.07×10^{-12}	0.307
G/WEP/WPU-0.1wt%	7.03×10^{-12}	0.323
G/WEP/WPU-0.3wt%	7.79×10^{-12}	-0.620
G/WEP/WPU-0.6wt%	8.50×10^{-12}	-0.381

To further elucidate the influence of graphene-modified oil-based epoxy/polyurethane composite on the corrosion resistance performance of the entire coating system, graphene content is plotted against the corrosion current density [Figure 7]. Figure 7 depicts the trend in the variation of corrosion current density of the modified oil-based epoxy/polyurethane composite coating with different graphene content. It is observed that when the content of the graphene added as corrosion inhibitor filler reaches 0.3 wt.%, the corrosion current density of the coating displays an obvious fall from 2.37×10^{-12} A/cm^2 to 1.81×10^{-12} A/cm^2. This fact may be attributed to the improvement in the surface quality of the epoxy primer facilitated by the addition of graphene and hence, the polyurethane topcoat can cure in a better way on its surface due to improved compatibility with the primer. These phenomena promote the formation of a relatively flat coating surface with fewer defects which can effectively hinder the penetration of corrosive media. However, when the content of graphene reaches 0.6 wt.%, the corrosion current density shows an increasing trend, indicating that the corrosion resistance starts to deteriorate. This phenomenon is induced by the granular protrusions on the surface of the coating (formed due to the aggregation of

graphene flakes) which increases the surface roughness. Corrosive media are found prone to deposit and accumulate on the electrode surface which leads to pitting corrosion in turn deteriorates the corrosion resistance performance of the coating.

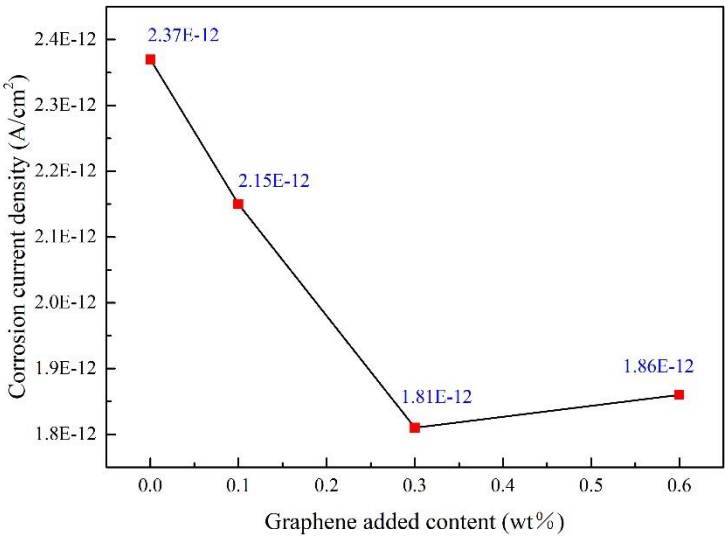

Figure 7. Variation in corrosion current density of graphene modified oil-based epoxy/polyurethane composite coatings with respect to different graphene content

Figure 8 shows the change in the corrosion current density of the graphene-modified waterborne epoxy/polyurethane composite coatings with respect to graphene content, which aids to understand the influence of graphene on the corrosion resistance of the waterborne composite coating. From Figure 8, it is clear that the addition of graphene doesn't reduce the corrosion current density of the coating but shows an increasing trend. When the added graphene content is 0.6 wt.%, the corrosion current density of the coated substrates increased from the initial 5.07×10^{-12} A/cm^2 to 8.50×10^{-12} A/cm^2. Along with interpretations from the surface microscopic images of the coating, it is believed that the primary cause for the decline in corrosion resistance property is that graphene preferentially agglomerates in the waterborne epoxy resin primer due to its strong hydrophobic property and the mutual attraction of the π-π bonds in the structure. The agglomeration weakens its property of being the filler for the structural defects in the coating that hinders its ability to block the corrosive media. As the primer surface becomes hydrophobic with a high degree of surface defects, uniform curing of waterborne polyurethane topcoat is not achieved. This leads to the decrease in the surface quality of the topcoat through high surface roughness and the occurrence of blistering. Corrosive media penetrates into the coating through these defects and causes damage. Thus, the overall corrosion resistance performance of the waterborne composite coating is found weakened.

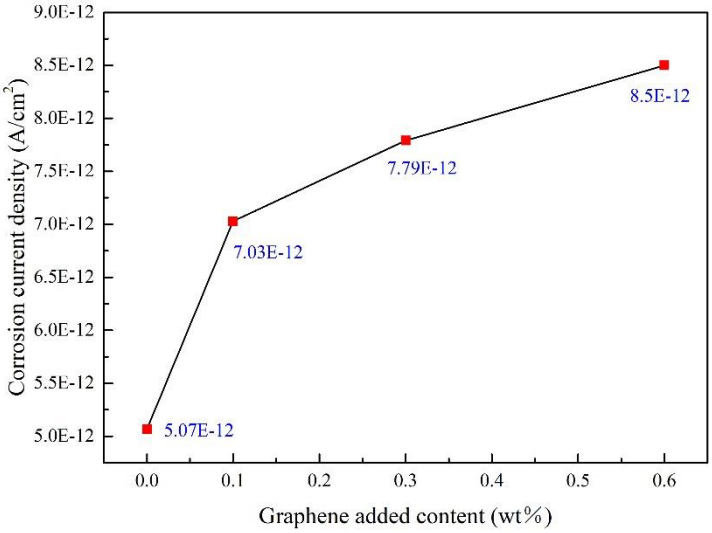

Figure 8. Variation in corrosion current density of graphene-modified waterborne epoxy/polyurethane composite coatings with respect to different graphene content

3.3. Analysis of coating corrosion mechanism

The microscopic surface morphologies of the graphene-modified oil-based epoxy/polyurethane composite coatings with different graphene content after electrochemical corrosion studies are shown in Figure 9. It is inferred from Figure 9(a) that the damage in the coating due to corrosion is more serious when graphene is not present because the penetration of corrosion ions into the coating is not hindered effectively. Damage phenomena such as pits, cracks, and peeling are introduced on the surface of the coating after corrosion. When 0.1 wt.% graphene is added, the corrosion resistance of the coating has been significantly improved where the formation of pits is restricted, depicted in Figure 9(b). This fact is attributed to the presence of graphene that improves the surface quality of the oil-based epoxy resin primer, in turn, promotes the oily polyurethane to form a good quality topcoat with a flat surface. Therefore, the deposition of corrosive media on the surface is prevented to a larger extent, and hence, the generation of pits is avoided. Nevertheless, owing to the low graphene content, failures such as cracks and pulverization caused by corrosion can be observed on the coating surface. With the further increase in graphene content to the primer, the surface morphology of the topcoat is found intact without cracking and chalking after electrochemical corrosion [Figure 9(c) & (d)]. However, slight granular protrusions are visible after the corrosion studies. When the graphene content is 0.3 wt.%, the surface of the oily composite coating displays the least morphological defects after corrosion with a relatively flat surface. So, the oily composite coated substrate shows the lowest corrosion current density value under this condition. As 0.6 wt.% graphene content is found to be high, graphene flakes tend to agglomerate in the primer that declines the surface quality by affecting the compatibility and curing quality of the topcoat which in turn declines the corrosion resistance. These interpretations further validate that when the graphene content is 0.3 wt.%, the coating shows the best corrosion resistance behavior.

There are very few reports similar to the coating system designed in the present work. However, it is evident from the literature related to the graphene-modified epoxy resin coating that the addition of

graphene can significantly reduce the internal defects of the coating [23-24]. Therefore, the pores on the surface of the coating are significantly reduced and the surface morphology is significantly improved. Subsequently, the corrosion resistance of the underlying metal is improved since the graphene addition prevents the corrosive medium to penetrate into the coating, and hence, the corrosion current density of the sample is significantly reduced as the graphene content increases. It is further verified from the present experimental studies that the graphene-modified oil-based epoxy resin primer can effectively cure the oily polyurethane topcoat on the surface of the primer that further improves the overall corrosion resistance of the composite coating.

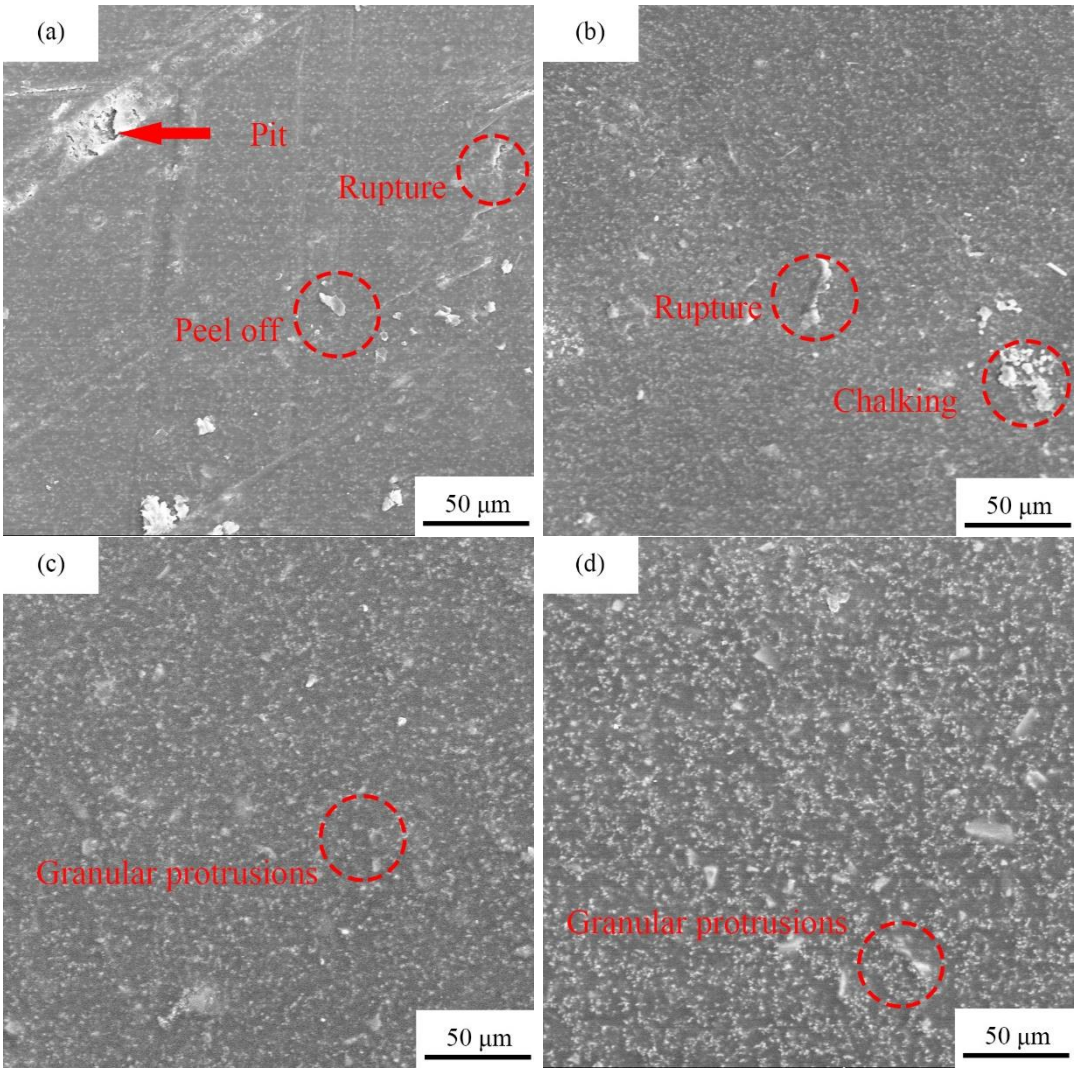

Figure 9. Surface morphologies of graphene-modified oil-based epoxy/polyurethane coatings after corrosion, (a) G/OEP/OPU-0wt%, (b) G/OEP/OPU-0.1wt%, (c) G/OEP/OPU-0.3wt%, and (d) G/OEP/OPU-0.6wt%

Figure 10 shows the microscopic surface morphologies of the graphene-modified waterborne epoxy/polyurethane composite coatings after electrochemical corrosion. It can be observed from the

figure that as the graphene content in the waterborne epoxy primer increases, the surface quality of the composite coating gradually decreases after corrosion. It validates that the corrosion resistance of the coating gradually weakens which corroborates with the same trend in the corrosion current density values of the waterborne composite coating as in the previous discussions. From the analysis, it is believed that the graphene will increase the hydrophobicity of the primer surface, causing uneven coating and curing of the waterborne polyurethane topcoat [Figure 10(a)]. When graphene is not added, the coating and curing effect of the waterborne polyurethane topcoat is obviously good, and thereby, the corrosive medium causes less damage to the surface of the coating. Therefore, the morphology of the surface after corrosion is relatively flat and no obvious defects are visible grading the waterborne composite coating without graphene content as the best. As the graphene content increases in the primer, the surface morphology of the composite coating becomes rough after corrosion. Even when the graphene content is 0.3 wt.%, apparent holes can be observed on the coating surface. When the graphene content is 0.6 wt.%, the porosity is further increased resulting in the significant reduction of corrosion resistance. This phenomenon is attributed to the ineffective coating and curing of the waterborne polyurethane topcoat on the cured hydrophobic primer surface which leads to poor cross-linking within the coating causing less dense coating. Therefore, the corrosive medium can effectively penetrate into the coating through these defects and cause corrosion.

As per the above discussions, although the addition of graphene will significantly improve the flatness of the epoxy resin coating and the diffusion resistance of the corrosive medium to the metal substrate, graphene is a highly hydrophobic material [25-27]. In a single-layer coating system, the graphene content increases the hydrophobicity of the coating surface and reduces the penetration of aqueous corrosive media into the coating. However, in the double-layer composite coating system (present work), the high degree of hydrophobicity of the graphene-modified primer may not allow the water-based polyurethane topcoat to adhere to the primer surface closely, resulting in weaker bonding between the coatings. This causes worsening surface defects on the topcoat and deteriorates the overall corrosion resistance of the waterborne composite coating.

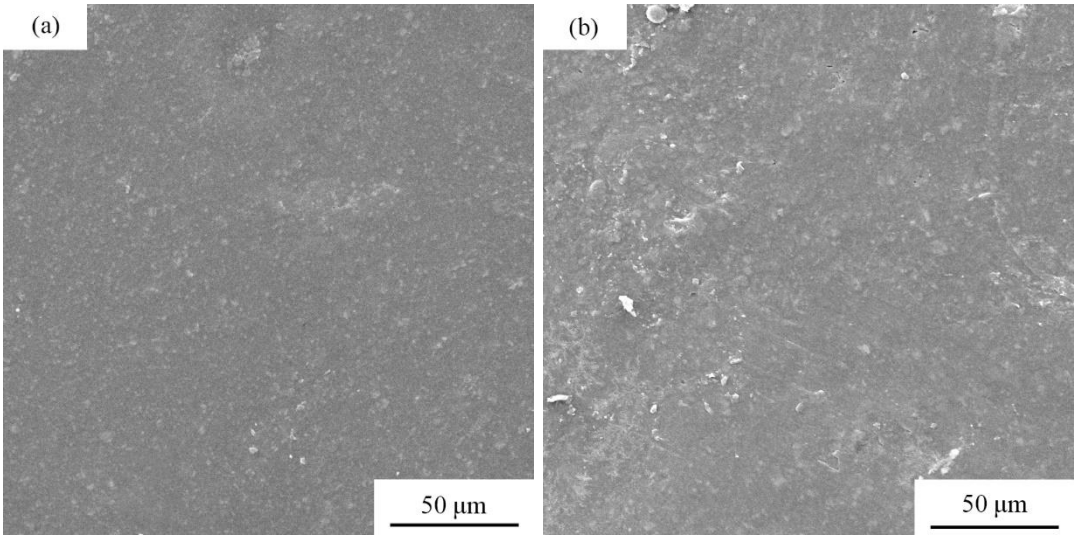

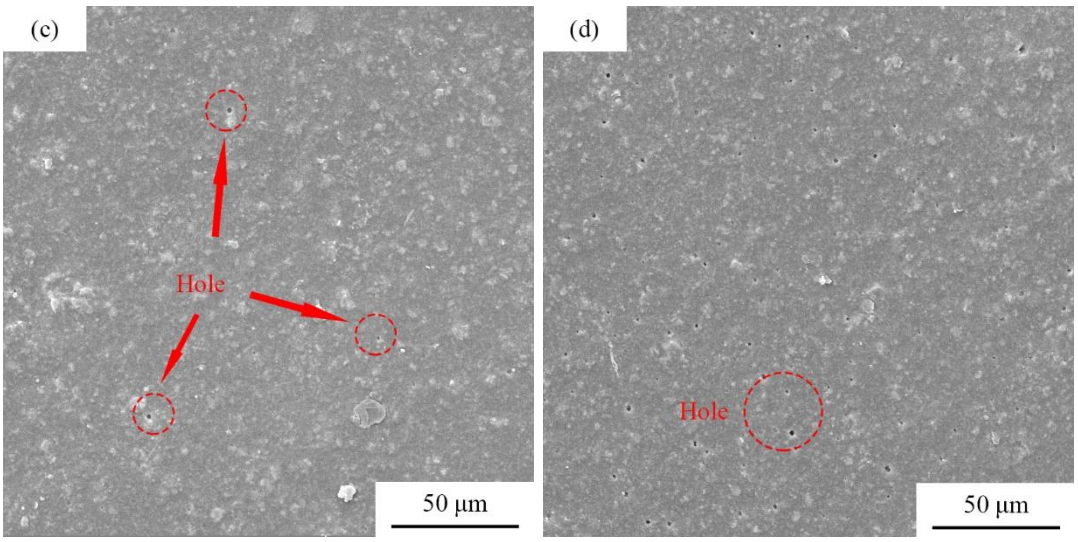

Figure 10. Corrosion morphologies of graphene-modified waterborne epoxy/polyurethane coatings, (a) G / WEP / WPU-0wt%, (b) G/WEP/WPU-0.1wt%, (c) G/WEP/WPU-0.3wt%, and (d) G/WEP/WPU-0.6wt%

4. CONCLUSIONS

The graphene-modified oily and waterborne epoxy/polyurethane composite coatings are prepared and coated over the surface of AZ31 magnesium alloy through brush coating technology. Graphene has fewer surface defects and is successfully impregnated into the epoxy primer through the stirring process. The corrosion current density of AZ31 magnesium alloy is 2.96×10^{-7}A/cm^2. Without graphene addition (0 wt.%), both G/OEP/OPU coating and G/WEP/WPU coating can improve the corrosion resistance of magnesium alloy. The graphene addition improves the bonding performance of the primer and topcoat in the G/OEP/OPU coating leading to the good surface quality of the topcoat in turn improves the corrosion resistance of the composite coating. When the graphene content is 0.3 wt.%, the composite coating displays its best corrosion resistance behavior where the corrosion current density is 1.81×10^{-12}A/cm^2. When graphene is added to the G/WEP/WPU coating, the hydrophobicity of graphene and the mutual attraction of the π-π bond will increase the surface hydrophobicity of the waterborne epoxy primer which hinders the effective curing of the waterborne polyurethane topcoat. Therefore, surface quality and the corrosion resistance of the waterborne composite coating are reduced. In this regard, G/WEP/WPU-0wt% is found to have the best corrosion resistance behavior among the waterborne composite coatings where the corrosion current density is 5.07×10^{-12} A/cm^2.

ACKNOWLEDGMENTS
This work is supported by the Science and Technology Research Program of Chongqing Municipal Education Commission(KJQN201800731) and the Scientific and Technological Research Program of Chongqing Science and Technology Bureau(cstc2019jcyj-msxmX0761, cstc2016jcyjA0424).

References

1. V. V. Ramalingam, P. Ramasamy, M. D. Kovukkal, G. Myilsamy, *Met. Mater. Int.,* 26 (2019) 409-430
2. S. Tekumalla, S. Seetharaman, A. Almajid, M. Gupta, *Metals*, 5 (2014) 1-39.
3. A. L. Rudd, C. B. Breslin, F. Mansfeld, *Corros. Sci.*, 42 (2000) 275-288
4. D. Seifzadeh, L. Farhoudi, *Surf. Eng*., 32 (2016) 348-355.
5. G. Song, *Adv. Eng. Mater.*, 7 (2005) 563-586.
6. Y. Chen, J. Li, W. Yang, S. Gao, R. Cao, *Appl. Surf. Sci.*, 493(2019) 1224-1235.
7. N. Palaniappan, I. S. Cole, F. Caballero-Briones, K. Balasubaramanian, C. Lal, *Rsc. Adv.*, 8 (2018) 34275-34286.
8. T. Jin, Y. Q. Han, R. Q. Bai, X. Liu, *J. Nanosci. Nanotechnol.,* 18 (2018) 4971-4981.
9. K. Y. Cao, Z. X. Yu, L. J. Zhu, D. Yin, L. G. Chen, Y. Jiang, J. Wang, *Surf. Coat. Tech.,*, 407(2021) 17.
10. Y. N. Chen, B. H. Ren, S. Y. Gao, R. Cao, J, *Colloid Interface Sci.*, 565 (2020) 436-448.
11. H. Tan, D. G. Wang, Y. B. Guo, *Anti-Corros. Method. M.*, 66 (2019) 853-860.
12. Y. Li, Z. Z. Yang, H. X. Qiu, Y. G. Dai, Q. B. Zheng, J. Li, J. H. Yang, *J. Mater. Chem. A*., 2 (2014) 14139-14145.
13. M. Hasani, M. Mahdavian, H. Yari, B. Ramezanzadeh, *Prog. Org. Coat.*, 11 (2018) 90-101.
14. S. Wang, R. Ding, X. D. Zhao, Q. Fu, H. Sun, S. Y. Chen, Z. Y. An, Y. Li, X. L. Qu, *Int. J. Electrochem. Sci.*, 15 (2020) 7082-7092.
15. H. Xu, H. J. Hu, H. M. Wang, Y. J. Li, Y. Li, *R. Soc. Open Sci.*, 7 (2020) 12.
16. J. Ding, H. Zhao, D. Ji, B. Xu, X. Zhao, Z. Wang, D. Wang, Q. Zhou, H. Yu, *J. Mater. Chem. A*., 7 (2019) 2864-2874.
17. S. Ren, M. Cui, W. Li, J. Pu, Q. Xue, L. Wang, *J. Mater. Chem. A*., 6 (2018) 24136-24148.
18. C. N. R. Rao, K. Biswas, K. S. Subrahmanyam, A. Govindaraj, *J. Mater. Chem.*, 19 (2009) 2457.
19. Y. Hao, Y. Wang, L. Wang, Z. Ni, Z. Wang, R. Wang, C. K. Koo, Z. Shen, J. T. Thong, *Small*, 6 (2010) 195-200.
20. T. Siva, K. Kamaraj, S. Sathiyanarayanan, *Prog. Org. Coat.,* 77 (2014) 1095-1103.
21. N. T. Duong, T. B. An, P. T. Thao, V. K. Oanh, T. A. Truc, P. G. Vu, T. T. X. Hang, *Vietnam J. Chem.*, 58 (2020) 108-112.
22. H. Y. Xu, D. Lu, X. Han, *Front. Mater. Sci.*, 14 (2020) 211-220.
23. C. H. Lu, C, Feng, L. J. Zhu, L. Jiang, G. H. Gao, L. H. Han, Y. R. Feng, *Adv.in Mater. Process.*, (2018). 1075-1082
24. Z. J. Liao, T. C. Zhang, S. Qiao, L. Y. H. Zhang, *IOP. Conf. Series. Earth. and. Environmental.*, 94 (2017) 012072.
25. T. Monetta, A. Acquesta, F. Bellucci, *Aerospace,* 2 (2015) 423-434.
26. H. Xu, H. J. Hu, H. M. Wang, Y. J. Li, Y. Li, *R. Soc. Open Sci.*, 7 (2020) 191943.
27. C. L. Chen, Y. He, G. Q. Xiao, F. Zhong, P. Xie, H. J. Li, L. He, *Colloid Surface A.*, 614 (2021) 126190.